Tunable Columnar Organization by Twisted Stacking of End-Capped Aromatic Rods

Zhegang Huang, Ja-Hyoung Ryu, Eunji Lee, and Myongsoo Lee*

The Center for Supramolecular Nano-Assembly and Department of Chemistry, Yonsei University, Seoul 120-749, Korea

The dumbbell-shaped aromatic amphiphilic molecules consisting of hexa-*p*-phenylene-conjugated carbazole moieties on both ends as a rigid rod segment and oligoether chains with different cross-sections (i.e., linear branch (**1**), dibranch (**2**), and tetrabranch (**3**)) attached to a carbazole as flexible chains were synthesized and their self-assembling behavior investigated using DSC, X-ray scatterings, and TEM. These dumbbell-shaped molecules based on an end-capped rod segment self-assemble into a tunable 2D supramolecular structure depending on cross-sectional area of the flexible dendritic chain. With increasing cross-sectional area of the flexible chains, the 2D structure changes from rectangular to oblique columnar structures with a successive increase in the lattice constant *a* relative to *b*. This structural change is also accompanied by increasing temperature as in the case of **2** and **3**. The molecular rearrangements at the phase transitions were proposed to undergo a scissoring motion of the two adjacent rods along the column axis. Considering that all other self-assembling systems based on rigid rod segments have a strong tendency to be aligned parallel to each other, the remarkable feature of the end-capped rod segment investigated in this study is the ability to control 2D supramolecular structure through a unique scissoring motion between the two adjacent stacked rods.

Introduction

A great deal of attention has been paid to the creation of supramolecular units through a self-assembly process of rationally designed molecules because of their wide application potentials in interdisciplinary areas combining chemistry, biology, and materials science.[1–4] Extensive efforts have thus been made to develop tunable and predictable supramolecular structures for exploration of novel properties and functions.[5–8]

Among self-assembling molecular systems, rod−coil block molecules provide a facile entry into this area.[9] Combining the immiscibility of incompatible segments and anisotropic arrangement of rod blocks renders complex organizational capability. With increasing the relative volume fraction of flexible chains, 2D layered structures break up into smaller domains, including cylinders and discrete bundles in which the rod segments are aligned parallel to each other.[10]

One can envision that the attachment of caps into both ends of a rod will frustrate a parallel arrangement of the rod segments commonly observed for linear rod−coil molecules, in order to minimize a steric repulsion between bulky segments. Instead, the rod segments can stack on top of each other with mutual rotation through microphase separation between incompatible molecular components and π−π stacking interactions of the aromatic units.[7] Consequently, this twisted packing enforces the rigid segments to grow in a one-dimensional way rather than conventional 2D growth.

* Corresponding author. Address: Center for Supramolecular Nano-Assembly and Department of Chemistry, Yonsei University, Shinchon 134, Seoul 120-749, Korea, Tel: 82-2-2123-2647. Fax: 82-2-393-6096. E-mail: mslee@yonsei.ac.kr.

(1) (a) Hoeben, F. J. M.; Jonkheijm, P.; Meijer, E. W.; Schenning, A. P. H. J. *Chem. Rev.* **2005,** *105,* 1491–1546. (b) Cornelissen, J. J. L. M.; Rowan, A. E.; Nolte, R. J. M.; Sommerdijk, N. A. J. M. *Chem. Rev.* **2001,** *101,* 4039–4070.

(2) (a) Ajayaghosh, A.; Vijayakumar, C.; Varghese, R.; George, S. J. *Angew. Chem., Int. Ed.* **2006,** *45,* 456–460. (b) Motoyanagi, J.; Fukushima, T.; Ishii, N.; Aida, T. *J. Am. Chem. Soc.* **2006,** *128,* 4220–4221. (c) Chen, B.; Baumeister, U.; Pelzl, G.; Das, M. K.; Zeng, X.; Ungar, G.; Tschierske, C. *J. Am. Chem. Soc.* **2005,** *127,* 16578–16591. (d) Antonietti, M.; Förster, S. *Adv. Mater.* **2003,** *15,* 1323–1333. (e) Li, L.-S.; Stupp, S. I. *Angew. Chem., Int. Ed.* **2005,** *44,* 1833–1836.

(3) (a) Ky Hirschberg, J. H. K.; Brunsveld, L.; Ramzi, A.; Vekemans, J. A. J. M.; Sijbesma, R. P.; Meijer, E. W. *Nature* **2000,** *407,* 167–170. (b) Kawano, S.-I; Fujita, N.; Shinkai, S. *J. Am. Chem. Soc.* **2004,** *126,* 8592–8593. (c) Kuroiwa, K.; Shibata, T.; Takada, A.; Nemoto, N.; Kimizuka, N. *J. Am. Chem. Soc.* **2004,** *126,* 2016–2021. (d) Percec, V.; Dulcey, A.; Balagurusamy, V. S. K.; Miura, Y.; Smidrkal, J.; Peterca, M.; Nummelin, S.; Edlund, U.; Hudson, S. D.; Heiney, P. A.; Duan, H.; Magonov, S. N.; Vinogradov, S. A. *Nature* **2004,** *430,* 764–768.

(4) (a) Kato, T; Mizoshita, N.; Kishimoto, K. *Angew. Chem., Int. Ed.* **2006,** *45,* 38–68. (b) Percec, V.; Aqad, E.; Peterca, m.; Rudick, J. G.; Lemon, L.; Ronda, J. C.; De, B. B.; Heiney, P. A.; Meijer, E. W. *J. Am. Chem. Soc.* **2006,** *128,* 16365–16372.

(5) (a) Enomoto, M.; Kishimura, A.; Aida, T. *J. Am. Chem. Soc.* **2001,** *123,* 5608–5609. (b) Moreau, L.; Barthelemy, P.; El Maataoui, M.; Grinstaff, M. W. *J. Am. Chem. Soc.* **2004,** *126,* 7533–7539.

(6) (a) Cuccia, L. A.; Ruiz, E.; Lehn, J.-M.; Homo, J.-C.; Schmutz, M. *Chem.−Eur. J.* **2002,** *8,* 3448–3457. (b) Ryu, J.-H.; Kim, H.-J; Huang, Z.; Lee, E.; Lee, M. *Angew. Chem., Int. Ed.* **2006,** *45,* 5304–5307.

(7) (a) Mori, A.; Yokoo, M.; Hashimoto, M.; Ujiie, S.; Diele, S.; Baumeister, U. Tschierske, C. *J. Am. Chem. Soc.* **2003,** *125,* 6620–6621. (b) Xu, Y.; Leng, S.; Xue, C.; Sun, R.; Pan, J.; Ford, J.; Jin, S. *Angew. Chem., Int. Ed.* **2007,** *46,* 3896–3899.

(8) (a) Kishimoto, K.; Suzawa, T.; Yokota, T.; Mukai, T.; Ohno, H.; Kato, T. *J. Am. Chem. Soc.* **2005,** *127,* 15618–15623. (b) Xu, Y.; Gu, W.; Gin, D. L. *J. Am. Chem. Soc.* **2004,** *126,* 1616–1617. (c) DePierro, M. A.; Carpenter, K. G.; Guymon, C. A. *Chem. Mater.* **2006,** *18,* 5609–5617.

(9) (a) Lee, M.; Cho, B.-K.; Zin, W.-C. *Chem. Rev.* **2001,** *101,* 3869–3892. (b) Lee, M.; Yoo, Y.-S. *J. Mater. Chem.* **2002,** *12,* 2161–2168.

(10) (a) Lee, M.; Cho, B.-K.; Jang, Y.-G.; Zin, W.-C. *J. Am. Chem. Soc.* **2000,** *122,* 7449–7455. (b) Ryu, J.-H.; Oh, N.-K.; Zin, W.-C.; Lee, M. *J. Am. Chem. Soc.* **2004,** *126,* 3551–3558.

Scheme 1. Synthesis of Dumbbell Shaped Aromatic Amphiphilic Molecules
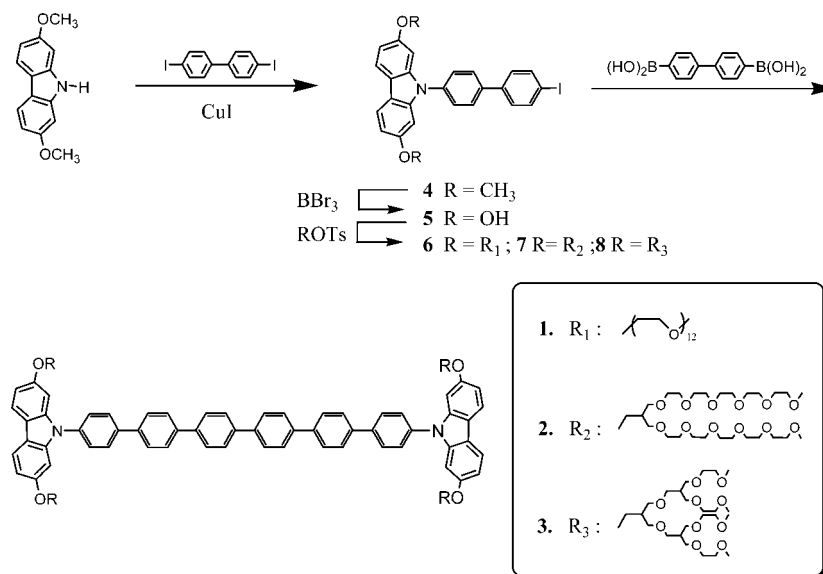
Thus, this design concept may offer an opportunity to manipulate 2D superlattice by controlling the twisted angle between the two neighboring stacked rods. With this consideration in mind, we have synthesized dumbbell-shaped block molecules based on an end-capped rod segment.

In this article, we present tunable 2D organizations of end-capped rod segments through π stacks in bulk. To frustrate a parallel arrangement of rod segments, we have designed dumbbell-shaped rigid–flexible block molecules consisting of an end-capped rigid rod segment and flexible oligoether chains with different cross-sections, that is linear branch (**1**), dibranch (**2**), and tetrabranch (**3**) (Scheme 1). And the self-assembly behavior was investigated in the bulk state by using optical polarized microscopy, differential scanning calorimetry (DSC), powder X-ray diffraction, and transmission electron microscopy (TEM). Because the rod:flexible chain volume ratio of the molecules is almost identical ($f_{rod} \approx 0.15$), the supramolecular structural variation can mainly be attributed to the different cross-sections of the flexible segments. As the cross-sectional area of flexible parts in the interface increases, the molecules showed to self-assemble successively into a 2D rectangular columnar, oblique columnar, and hexagonal columnar structure.

Results and Discussion

Synthesis. The synthesis of molecular dumbbell **1**–**3** consisting of a carbazole end-capped hexa-*p*-phenylene as a rigid stem and flexible oligoether segments laterally attached to carbazole units as flexible chains starts with the preparation of 2,7-dimethoxycarbazole and polyether dendrons according to the procedures described previously.[11,12] To control the cross-sectional area of the flexible chain at the fixed rod volume fraction ($f_{rod} \approx 0.15$), the design of dendritic side chains was focused on poly(ethylene glycol) monomethyl

ether (DP = 12) (linear branch), penta(ethylene glycol) monomethyl ether (dibranch), mono(ethylene glycol) monomethyl ether (tetrabranch). *N*-Aryl-substituted carbazole derivative **4** was prepared from the coupling with 4,4′-diiodobiphenyl by using CuI as a catalysis. For the next reaction, the methoxy groups of **4** were deprotected, and the subsequent etherification with tosylated polyether dendrons then yielded **6**, **7**, and **8.** The final molecules were synthesized by Suzuki coupling reaction of **6**, **7**, and **8** with 4,4′-biphenyldiboronic acid.

The resulting molecules **1**–**3** were characterized by ^{1}H and ^{13}C NMR spectroscopy and matrix-assisted laser desorption ionization time-of-flight (MALDI-TOF) mass spectroscopy and were shown to be in full agreement with the structures presented. As confirmed by ^{1}H NMR spectroscopy, the ratio of the aromatic protons of the rod block to the alkyl protons is consistent with the ratio calculated, and the MALDI-TOF mass spectra of the molecules exhibit two or three signals that can be assigned as the H$^+$-, Na$^+$-, and K$^+$-labeled molecular ions. The mass corresponding to a representative peak in the spectrum is matched with the calculated molecular weight of each molecule.

Bulk State Structure. All of the molecules showed an ordered bulk-state structure that is thermodynamically stable, as verified by the heating and cooling DSC scans, and the transition temperatures and the corresponding enthalpy changes are summarized in Table 1. To investigate the bulk-state structure of the dumbbell-shaped molecules, we performed X-ray scattering experiments at various temperatures. The X-ray diffraction pattern of **1** displayed a number of sharp reflections including several equidistant peaks, indicative of the existence of a long-range-ordered structure (Figure 1). These reflections could be indexed as a 2D primitive rectangular columnar structure with lattice parameters $a = 1.9$ nm, $b = 3.8$ nm, and $c = 1.2$ nm.

Both molecules **2** and **3** showed a number of sharp reflections at room temperature, again indicative of the existence of a highly ordered nanoscopic structure. In contrast to **1**, however, the primary peak showed to shift to a higher

(11) Freeman, A. W.; Urvoy, M.; Criswell, M. E. *J. Org. Chem.* **2005**, *70*, 5014–5019.

(12) Jayaraman, M.; Frechet, J. M. J. *J. Am. Chem. Soc.* **1998**, *120*, 12996–12997.

Table 1. Thermal Transitions of Dumbbell-Shaped Molecules (data are from heating and cooling scans)[a]

molecules	ρ^b (g/cm^3)	$f_{rod}{}^c$	heating	cooling
			phase transition (°C) and corresponding enthalpy changes (kJ/mol)	
1	1.15	0.15	r-col 135.5(25.7) i	i 110.6(22.8) r-col
2	1.14	0.15	o-col 35.9(6.2) o-col 43.3(1.6) h-col 66.5(9.4) i	i 53.5(8.5) h-col 40.8(2.3) o-col 27.9(5.9) o-col
3	1.13	0.17	o-col 37.2(1.8) h-col 118.8(7.4) i	i 106.4(9.0) h-col 34.9(0.3) o-col

[a] r-col, rectangular columnar; o-col, oblique columnar; h-col, hexagonal columnar. [b] ρ = molecular density. [c] f_{rod} = rod volume fraction.
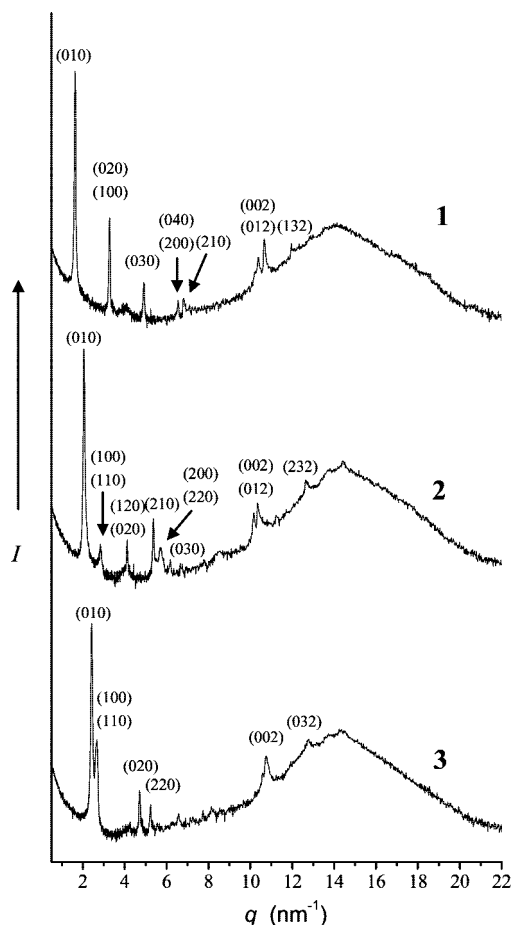
Figure 1. X-ray diffraction patterns of **1**−**3** plotted against q (= $4\pi \sin 2\theta/\lambda$) at room temperature. The rectangular columnar lattice exhibited by **1** and the oblique columnar lattice exhibited by **2** and **3**.

Figure 2. TEM images of ultramicrotomed films of (a) **1**, (b) **2**, and (c) **3** stained with RuO$_4$ revealing an ordered array of alternating light-colored dendritic layers and dark aromatic layers. The inset images of (b) and (c) at perpendicular beam incidence show an obliquely ordered array of aromatic core (scale bar = 10 nm).

from X-ray scattering. Similar to **2**, TEM images of **3** also showed an oblique columnar array in which the ratio of two characteristic dimensions (a/b) is close to unity.

To better understand the packing arrangement, we calculated the number (n) of molecules in a unit cell of the column. Calculated from the lattice constants determined from X-ray patterns and measured densities, the average number (n) of molecules in a unit cell was estimated to be approximately 2 in all the molecules (Table 2).[13] Interestingly, lattice constant c (= 1.2 nm) values that originate from the π stacking distance between neighboring rods are identical in all cases, as shown in Figure 1. On the basis of these results, we consider that the two molecules in a unit cell are stacked along the c axis with mutual rotation to minimize a steric repulsion between bulky dendritic segments. Consequently, the rod segments aggregate in one dimension with an ABAB arrangement through microphase separation between incompatible molecular components and $\pi-\pi$ stacking interactions between the aromatic units (Figure 3). The resulting 1D aggregates self-organize into 2D columnar structures with different a to b ratios depending on the cross-section of the flexible chain (Table 2).

Considering that the volume fractions of the flexible chains are almost identical in all the molecules ($f_{rod} \approx 0.15$), this variation in the a/b ratio seems to be attributed to the different twisted angles between two neighboring stacked rods. With increasing cross-sectional area of the flexible chains, steric repulsions between bulky dendritic segments at both ends of the rods increases, resulting in energetic penalty associated with chain deformation. To relieve the steric repulsions without sacrificing π-stacking interactions between the rods, the rod would rotate with respect to its neighbor at a fixed interrod $\pi-\pi$ stacking distance to produce a larger twisted angle. Note that all of the X-ray scattering patterns, regardless of molecular architecture, showed a (002) reflection at the same position, indicating that the distance of the two

angle, and a new peak next to the primary peak was identified. These reflections could be indexed as a 2D oblique columnar structure with a characteristic angle of $\gamma = 69$ and 62°, and lattice parameters $a = 2.3$ nm, $b = 3.3$ nm, $c = 1.2$ nm and $a = 2.7$ nm, $b = 2.9$ nm, $c = 1.2$ nm for **2** and **3**, respectively.

To further confirm the formation of a 2D structure, we cryomicrotomed dumbbell-shaped molecules **1**–**3** to a thickness of ca. 50–70 nm; we then stained them with RuO$_4$ vapor and observed them by transmission electron microscopy (TEM). As shown in Figure 2a, TEM image of **1** showed organized 1D dark domains with a thickness of 3.8 nm, which is identical to the value from X-ray scattering. The micrograph of **2** showed organized 1D dark, more stained aromatic domains. Inset TEM image showed in-plane order of an oblique symmetry in which dark rod domains are regularly arrayed in a light flexible chain matrix. The interdomain distances were measured to be approximately 2.3 and 3.3 nm, which are consistent with those obtained
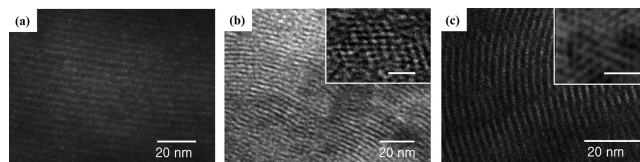
(13) From the experimental values of the intercolumnar distance (a, b), and the densities (ρ), the average number (n) of molecules arranged in a unit cell of the cylinders with a thickness (c) of 12 Å (as observed from X-ray diffraction) can be calculated according to following equation, where M is the molecular mass and N_A is Avogadro's number: $n = abc \sin(\gamma) (N_A/M)\rho$.

Table 2. Characterization of Dumbbell-Shaped Molecules by X-ray Scattering

| | rectangular columnar | | | | | oblique columnar | | | | | oblique columnar | | | | | hexagonal columnar | | | | | |
| | lattice constant[a] | | | | | lattice constant[a] | | | | | lattice constant[a] | | | | | lattice constant[a] | | | | | |
molecule	a	b	c	γ	a/b	a	b	c	γ	a/b	a	b	c	γ	a/b	a	c	γ	a/b	twisted angle (deg)[b]	n[c]
1	1.9	3.8	1.2	90	0.50															35	2
2						2.3	3.3	1.2	69	0.71	2.7	3.0	1.2	64	0.91	2.9	1.2	60	1	70	2
3											2.7	2.9	1.2	62	0.91	2.9	1.2	60	1	82	2

[a] The lattice constants (nm) and the characterized angles (deg). [b] Twisted angle of neighborng molecules from computer model. [c] The number n of molecules in a unit cell.
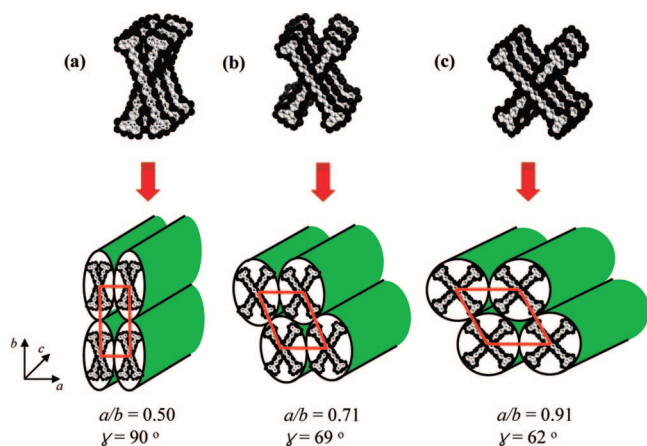

Figure 3. Schematic representation of 2D organization of (a) **1**, (b) **2**, and (c) **3**. Flexible chains were omitted for clarify.
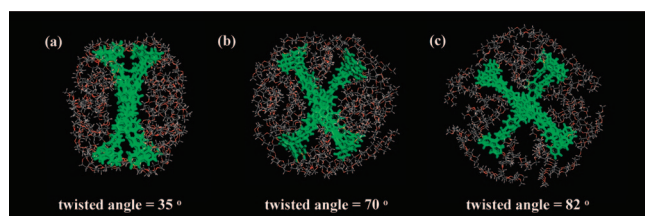

Figure 4. Front view of twist arrangements by molecular modeling of (a) **1**, (b)**2**, and (c) **3** (rod segments are colored green, oxygens and hydrocarbons are colored red and grey, respectively).

Figure 5. Fluorescence spectra of (a) molecule **1** in CHCl₃ solution, (b) solid film of molecule **1**, (c) solid film of molecule **2**, and (d) solid film of molecule **3**.

neighboring stacked rods is fixed to 6.0 Å. This twisted angle variation gives rise to the shape change of columnar slice from ellipse to circle, which is consistent with an increase in the *a/b* ratio of the 2D columnar structure (Table 2). This increase in the interrod angle is reflected in the gradual increase of the lattice constant *a* relative to *b* with increasing the cross-section of the flexible chain. Consequently, the cross-section of the column became more and more circular in shape, resulting in the transformation from rectangular, oblique to hexagonal columnar structure (Table 2). This effect is illustrated by a computer model in which the COMPASS empirical force-field calculation is used on a small cluster of six molecules stacked on top of each other with a center to center distance of 6 Å obtained from the X-ray results (lattice constant *c*) (Figure 4). Energy minimization of the cluster suggests that a twist arrangement of the rod segments is energetically favorable. The calculation revealed that the neighboring rods in a column are twisted to each other in ABAB arrangement along the *c* axis with angles of about 35, 70, and 82° for **1**, **2**, and **3**, respectively. Considering that the π stacking distance between the two rods remains unchanged, the variation in cross-sectional area of the flexible chain drives the rod segments to adopt a
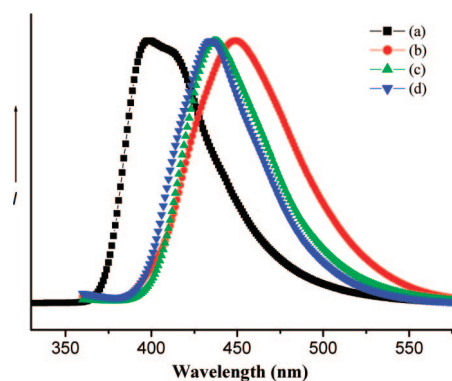
molecular rearrangement through a scissoring motion within the columnar core. Consequently, this rearrangement of the rods seems to be responsible for the supramolecular structural change in two dimensions.

To gain further insight into the molecular arrangements within one column, we have performed steady-state fluorescence spectroscopy experiments with the molecular dumbbells (Figure 5). The wavelength of maximum emission (λ_{max}) of **1** in dilute solution is 397 nm, but the bulk-state fluorescence spectra of **1**, **2**, and **3** show a strong maximum between 430 and 450 nm, suggesting that the band comes from π stacking of the rod building block.[14,15] The emission maxima appeared to be 449, 437, and 434 nm for **1**–**3**, respectively, indicating that the emission maximum gradually shift to higher energy as the cross-section of the flexible chains increases. Considering that the π-stacking distance remains unaltered with a cross-sectional area change of the flexible chains, this trend could be attributed to the extent of π-stacking overlap between adjacent rods,[16] which is consistent with a proposed scissoring motion in supramolecular structural variation.

Interestingly, this structural change was also observed by temperature variation as in the case of **2** and **3**. Both molecules have multiple phase transitions as confirmed by DSC scans (Table 1). As mentioned previously, molecule **2** at room temperature self-assembles into an oblique columnar structure with elliptical columnar slice in shape. On heating,

(14) McQuade, D. T.; Kim, J.; Swager, T. M. *J. Am. Chem. Soc.* **2000**, *122*, 5885–5886.

(15) Lee, M.; Jeong, Y.-S.; Cho, B.-K.; Oh, N.-K.; Zin, W.-C. *Chem.—Eur. J.* **2002**, *8*, 876–883.

(16) (a) Brédas, J.-L.; Beljonne, D.; Coropceanu, V.; Cornil, J. *Chem. Rev.* **2004**, *104*, 4971–5003. (b) Janzen, D. E.; Burand, M. W.; Ewbank, P. C.; Pappenfus, T. M.; Higuchi, H.; da Silva Filho, D. A.; Young, V. G.; Brédas, J.-L.; Mann, K. R. *J. Am. Chem. Soc.* **2004**, *126*, 15295–15308.
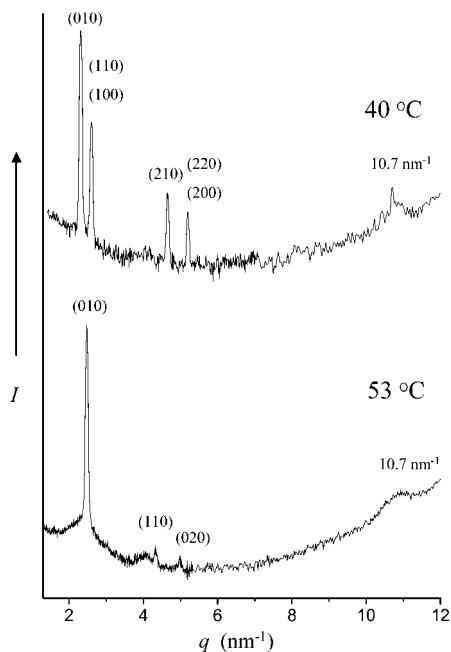
Twisted Stacking of End-Capped Aromatic Rods

Chem. Mater., Vol. 19, No. 26, 2007 6573

Figure 6. X-ray diffraction patterns measured at different temperatures plotted against q ($= 4\pi \sin 2\theta/\lambda$) in the oblique columnar structure at 40 °C, and the hexagonal columnar structure at 53 °C for **2**.

the X-ray pattern showed a number of well-resolved reflections, which can be indexed as a 2D oblique columnar lattice with lattice parameters $a = 2.7$ nm, $b = 3.0$ nm, and $\gamma = 64°$ (Figure 6). Compared to the room temperature X-ray pattern, the (100) peak is shifted toward the primary peak (010) with an increase in the a/b ratio, whereas a decrease in characteristic angle (γ). These results demonstrate that the elliptical shape of the columnar slice changes to be more circular with increasing temperature. With further heating, the oblique columnar structure transforms into a hexagonal columnar structure with a lattice constant $a = 2.9$ nm. On slow cooling from the isotropic liquid, the formation of pseudofocal conic domains that typical texture of hexagonal columnar could be observed between crossed polarizers.[17] It is interesting to note that all of the X-ray scattering patterns, regardless of temperature, showed a reflection at the same position, a q-value of about 10.7 nm^{-1}, indicating that the π stacking distance between the two neighboring rods remains to be unchanged with temperature variation.

These results demonstrate that the 2D supramolecular structure changes from oblique to hexagonal columnar structures on heating, which is accompanied by increasing the lattice constant a relative to b with the π stacking distance between the adjacent rods remaining unaltered. On heating, higher thermal motion of flexible chains relative to that of the stiff-rod segments requires a larger interfacial area to reduce enhanced space crowding in the flexible domains.[18,19] This spatial requirement enforces the stacked rods being more rotated to each other with a larger twisted angle. Eventually, the lattice constant ratio (a/b) of the 2D oblique lattice

(17) See the Supporting Information.
(18) (a) Lee, M.; Cho, B.-K.; Kim, H.; Yoon, J.-Y.; Zin, W.-C. *J. Am. Chem. Soc.* **1998**, *120*, 9168–9179. (b) Lee, M.; Cho, B.-K.; Kim, H.; Zin, W.-C. *Angew. Chem., Int. Ed.* **1998**, *37*, 638–640.
(19) Chen, B.; Zeng, X. B.; Baumeister, U.; Diele, S.; Ungar, G.; Tschierske, C. *Angew. Chem., Int. Ed.* **2004**, *43*, 4621–4625.
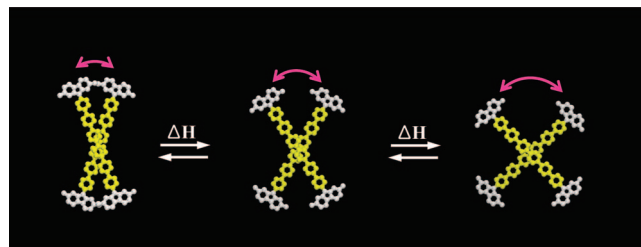
Figure 7. Schematic representation of a reversible scissoring motion triggered by temperature of the molecular dumbbell **2**.

increases to transform into a 2D hexagonal columnar structure. These results imply that the two adjacent stacked rods undergo reversible molecular rearrangements through a scissoring motion by changing temperature (Figure 7). **3** based on the tetra-branched dendrons shows a similar thermal behavior. The oblique columnar structure with two characteristic dimensions transforms on heating into a hexagonal columnar structure with a lattice constant $a = 2.9$ nm (Table 2). Again, this structural change indicates that the angle between the two stacked rods within the aromatic core reversibly increases through a scissoring motion on heating to relieve the steric hindrance between the bulky dendritic chains with higher thermal motion.

Aggregation Behavior in Aqueous Solution. The dumbbell-shape molecules **1**–**3**, when dissolved in a selective solvent for one of the blocks, can self-assemble into an aggregate structure because of their amphiphilic characteristics.[20–22] The aggregation behaviors of these molecules were subsequently studied in aqueous solution using UV−vis and fluorescence spectra. The absorption spectrum of **2** in aqueous solution (0.002 wt %) exhibits a broad transition with a maximum at 350 nm, resulting from the conjugated rod block (Figure 8a). The fluorescence spectrum of **2** in chloroform solution (0.002 wt %) exhibits a strong emission maximum at 397 nm. However, the emission maximum in aqueous solution is red-shifted with respect to that observed in chloroform solution, and the fluorescence is significantly quenched, indicative of aggregation of the conjugated rod core segments.[23,24] Dynamic light scattering (DLS) experiments were performed with **2** in aqueous solution (0.01 wt %) to further investigate the aggregation behavior (Figure 8b). CONTIN analysis of the autocorrelation function shows a broad peak ranging from several nanometers to hundreds

(20) (a) Yoo, Y.-S.; Choi, J.-H.; Song, J.-H.; Oh, N.-K.; Zin, W.-C.; Park, S.; Chang, T.; Lee, M. *J. Am. Chem. Soc.* **2004**, *126*, 6294–6300. (b) Discher, D. E.; Eisenberg, A. *Science* **2002**, *297*, 967–973. (c) Förster, S.; Plantenberg, T. *Angew. Chem., Int. Ed.* **2002**, *41*, 688–714.
(21) (a) Zhang, G.; Jin, W.; Fukushima, T.; Kosaka, A.; Ishii, N.; Aida, T. *J. Am. Chem. Soc.* **2007**, *129*, 719–722. (b) Kim, B.-S.; Hong, D.-J.; Bae, J.; Lee, M. *J. Am. Chem. Soc.* **2005**, *127*, 16333–16337. (c) Xu, J.; Zubarev, E. R. *Angew. Chem., Int. Ed.* **2004**, *43*, 5491–5496.
(22) (a) Ornatska, M.; Peleshanko, S.; Genson, K. L.; Rybak, B.; Bergman, K. N.; Tsukruk, V. V. *J. Am. Chem. Soc.* **2004**, *126*, 9675–9684. (b) Niece, K. L.; Hartgerink, J. D.; Donners, J. J. J. M.; Stupp, S. I. *J. Am. Chem. Soc.* **2003**, *125*, 7146–7147.
(23) (a) Ajayaghosh, A.; George, S. J. *J. Am. Chem. Soc.* **2001**, *123*, 5148–5149. (b) Hoeben, F. J. M.; Shklyarevskiy, I. O.; Pouderoijen, M. J.; Engelkamp, H.; Schenning, A. P. H. J.; Christianen, P. C. M.; Maan, J. C.; Meijer, E. W. *Angew. Chem., Int. Ed.* **2006**, *45*, 1232–1236.
(24) (a) Bae, J.; Choi, J.-H.; Yoo, Y.-S.; Oh, N.-K.; Kim, B.-S.; Lee, M. *J. Am. Chem. Soc.* **2005**, *127*, 9668–9669. (b) Messmore, B. W.; Hulvat, J. F.; Sone, E. D.; Stupp, S. I. *J. Am. Chem. Soc.* **2004**, *126*, 14452–14458. (c) Varghese, R.; George, S. J.; Ajayaghosh, A. *Chem. Commun.* **2005**, 593–595.
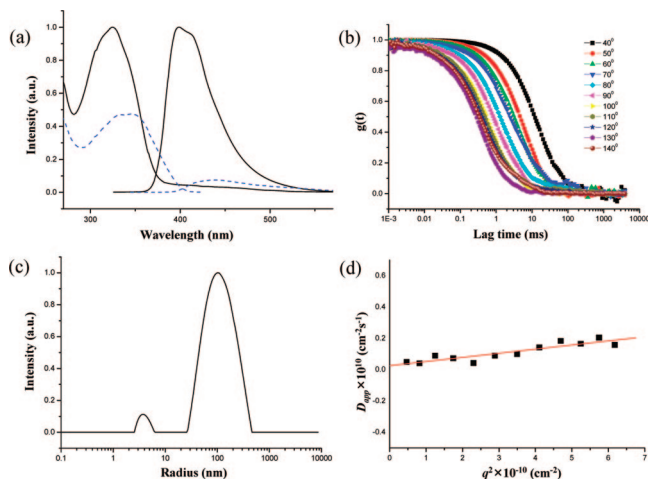
Figure 8. (a) Absorption and emission spectra of **2** in CHCl₃ (0.002 wt %, black line) and aqueous solution (0.002 wt %, blue dot line). (b) Autocorrelation functions of **2** in aqueous solution (0.01 wt %). (c) Hydrodynamic radius distribution of **2**. (d) Angular dependence of diffusion coefficient for **2**.
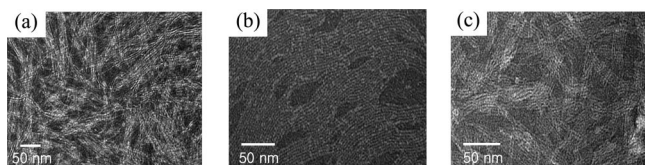

Figure 9. TEM images (negatively stained with uranyl acetate) of sample cast from aqueous solution of (a) **1**, (b) **2**, and (c) **3**.

nanometers (Figure 8c). The angular dependence of the apparent diffusion coefficient (D_{app}) was measured because the slope is related to the shape of the diffusing species. As shown in Figure 8d, the slope was observed to be 0.026, consistent with the value predicted for elongated nonspherical micelles (0.03).[25] Compounds **1** and **3** showed similar aggregation behavior to that of **2**, and their R_h value showed to be 155 and 61 nm, respectively.

The evidence for the formation of the cylindrical aggregates was also provided by transmission electron microscopy (TEM) experiments (Figure 9). TEM micrographs of **2** clearly show cylindrical aggregates with a uniform diameter of about 4.3 nm. Considering the extended molecular length (7.7 nm by CPK modeling), the image indicates that the

(25) Schmidt, M.; Stockmayer, W. H. *Macromolecules* **1984**, *17*, 509–514.

diameter of the elementary cylindrical objects corresponds to one molecular length. Remarkably, compounds **1** and **3** also self-assemble to cylindrical micelles with a uniform diameter of 5.4 and 3.9 nm, respectively. These results suggest that the cylindrical aggregates consist of aromatic cores surrounded by hydrophilic chains in which the rod segments stack on top of each other with irregular rotation.

Conclusions

The results described here demonstrate that the dumbbell-shaped molecules based on an end-capped rod segment self-assemble into 2D supramolecular structures with a variable a/b ratio depending on the cross-sectional area of the flexible dendritic chain. As the cross-sectional area of the flexible chain increases, the organized 2D structure changes from a rectangular columnar structure to an oblique columnar structure with increasing the lattice constant a relative to b. This supramolecular structural change in two dimensions is also caused by increasing temperature as in the case of **2** and **3**. Therefore, changing temperature produces a similar effect to varying the cross-sectional area of grafted flexible chains. The primary driving force responsible for this structural change is believed to be twisted stacking of the end-capped rod segments with mutual rotation along the column axis and subsequent space-filling requirement of flexible chains. The molecular rearrangements of the end-capped rod segments at the phase transitions can be considered to undergo through a scissoring motion of the two neighboring rods along the column axis. In the same context, this molecular scissoring motion undergoes in a reversible way with varying temperature as evidenced by the thermal behavior of **2**. In dilute aqueous solution, the molecules were observed to self-assemble into cylindrical micelles.

Supporting Information Available: Experimental section; Tables S1−S6; Figures S1−S4 (PDF). This material is available free of charge via the Internet at http://pubs.acs.org.

CM7028189